What we can learn from measurements of air electric conductivity in 222Rn-rich atmosphere

Elena Seran, Michel Godefroy, Éric Pili, Nathalie Michielsen, Sylvain Bondiguel

AGU PUBLICATIONS

Earth and Space Science

RESEARCH ARTICLE
10.1002/2016EA000241

Key Points:
- New design of instrument to measure electric conductivity of air in high and variable electric field is proposed (Mars application)
- Performances of new instrument to measure electric conductivity of air were tested in ^{222}Rn-rich environments
- An analytical model is proposed with intention to explain the measured values of the air electric conductivity at different ^{222}Rn activity concentrations

Correspondence to:
E. Seran,
seran@latmos.ipsl.fr

Citation:
Seran, E., M. Godefroy, E. Pili, N. Michielsen, and S. Bondiguel (2017), What we can learn from measurements of air electric conductivity in ^{222}Rn-rich atmosphere, *Earth and Space Science*, *4*, 91–106, doi:10.1002/2016EA000241.

Received 14 NOV 2016
Accepted 13 JAN 2017
Accepted article online 19 JAN 2017
Published online 23 FEB 2017

What we can learn from measurements of air electric conductivity in ^{222}Rn-rich atmosphere

E. Seran[1], M. Godefroy[1], E. Pili[2], N. Michielsen[3], and S. Bondiguel[3]

[1]LATMOS/IPSL/UVSQ/UPMC, Paris, France, [2]CEA, DAM, DIF, Arpajon, France, [3]IRSN, Saclay, Gif-sur-Yvette, France

Abstract Electric conductivity of air is an important characteristic of the electric properties of an atmosphere. Testing instruments to measure electric conductivity ranging from ~10^{-13} to 10^{-9} S m^{-1} in natural conditions found in the Earth atmosphere is not an easy task. One possibility is to use stratospheric balloon flights; another (and a simpler one) is to look for terrestrial environments with significant radioactive decay. In this paper we present measurements carried out with different types of conductivity sensors in two ^{222}Rn-rich environments, i.e., in the Roselend underground tunnel (French Alps) and in the Institute of Radioprotection and Nuclear Safety BACCARA (BAnC de CAllibrage du RAdon) chamber. The concept of the conductivity sensor is based on the classical time relaxation method. New elements in our design include isolation of the sensor sensitive part (electrode) from the external electric field and sensor miniaturization. This greatly extends the application domain of the sensor and permits to measure air electric conductivity when the external electric field is high and varies from few tens of V m^{-1} to up to few tens of kV m^{-1}. This is suitable to propose the instrument for a planetary mission. Two-fold objectives were attained as the outcome of these tests and their analysis. First was directly related to the performances of the conductivity sensors and the efficiency of the conductivity sensor design to shield the external electric field. Second objective aimed at understanding the decay mechanisms of ^{222}Rn and its progeny in atmosphere and the impact of the enclosed space on the efficiency of gas ionization.

1. Introduction

Earth's atmosphere represents a unique natural laboratory that offers a large variety of electric conditions and also multiple mechanisms which control its electrical features [*Seran et al.*, 2013]. From the ground to the upper stratosphere, the electric conductivity of air gradually grows from ~10^{-14} to ~10^{-10} S m^{-1}, while the vertical electric field decreases from ~100 V m^{-1} to ~10 mV m^{-1}. Locally, during short time periods and in extreme meteorological conditions (thunderstorms or dust activation phenomena), the electric field can grow up to ~10–100 kV m^{-1}.

Electric conductivity of the atmosphere, which characterizes its ability to conduct an electric current, is defined by the concentration of light ions of both polarities in the atmosphere and their mobility. Among the natural sources of air ionization, the most efficient are (i) short wavelength ultraviolet (UV) emissions, (ii) cosmic rays, and (iii) radioactive isotopes. In the Earth's atmosphere, the efficiency of these sources varies typically with altitude. The extreme UV is almost entirely absorbed in the upper atmosphere, while the interaction of cosmic rays with the atmosphere mainly takes place in the lower stratosphere-troposphere and results in extensive cascade of ionized particles and electromagnetic radiations. ^{222}Rn gas naturally exhales from soils or rocks and then decays in air. It may occasionally become a concurrent ionization source near the ground and often a major source in confined underground spaces, particularly in U-rich environments such as in cavities hosted in granitic rocks.

Such a variety of ionization sources existing in the near Earth environment offers numerous possibilities to test the instrumental concepts of conductivity sensors. For example, similar and relatively high values of the air electric conductivity may be found in a low-pressure stratosphere or in an underground cavity like the dead-end tunnel of the Roselend Natural Laboratory (French Alps). There, electric conductivity of air may locally change its magnitude during temporal intervals up to several weeks, in association with variations in the ^{222}Rn gas fluxes emitted from the surrounding rocks, combined with natural ventilation and decay [*Richon et al.*, 2005]. Desired amplitudes of air electric conductivity can also be reproduced in the laboratory, using confined chambers equipped with an ionization source (extreme UV lamp, ^{222}Rn gas, etc.). Laboratory facilities offer stationary and controlled conditions of gas ionization associated with the choice of different

gas pressures and types of injected gas. In the BACCARA chamber of the Institute of Radioprotection and Nuclear Safety (IRSN), the established ^{222}Rn activity concentrations are traceable to a primary ^{222}Rn gas standard [*Michielsen and Voisin*, 1999; *Picolo et al*., 2000; *Röttger et al*., 2006].

The instruments that were tested in ^{222}Rn-rich environments are conductivity sensors developed to measure the electric conductivity of air by means of the commonly used time relaxation method [see, e.g., *Mozer and Serlin*, 1969]. One of the limitations of this method is that the electric field produced by the potential applied to the electrode in the initial phase of the relaxation measurements has to be significantly higher than the ambient DC and AC (continuous and alternative) electric field. This constraint does not create any problems for measurements made in the quiet Earth's stratosphere with electric field of a fraction of Vm^{-1}, but it does if the instrument is used on Mars surface where the electric field is expected to be highly variable and may attain ~few kVm^{-1} (inside dust devils). A new design of the conductivity sensor that we developed and present in this paper allows to overcome the above mentioned problem. In this design, the sensitive part of the sensor continues to stay in contact with air but is isolated from the external electric field by an electrically grounded grid. Performances of this instrument, hereafter called conductivity sensor-2 (or CS-2), are assessed and compared with the performances of a simple electrode, hereafter called conductivity sensor-1 (or CS-1).

The structure of this paper is the following. We start in section 2 with description of the instrumental concept; propose a simplified electric schematic of the conductivity sensors and a method to calculate the air electric conductivity from the measured coupling resistance. Brief descriptions of the Roselend tunnel and BACCARA chamber are given in section 3. An analytical model developed to establish the relationship between ^{222}Rn activity concentration and electric conductivity of air is presented in section 4. A solution is given for stationary conditions and takes into account the ion sink and loss of alpha particles on the walls of the enclosed space. This solution is applied in section 5 to fit the air electric conductivity measured in the BACCARA chamber at different levels of the ^{222}Rn activity concentration and gas pressure. In section 6, two series of measurements performed in the Roselend tunnel are displayed and discussed. The aim of the first observational sequence, performed simultaneously with the two conductivity sensors, was to demonstrate the efficiency of the CS-2 design to shield an external electric field. The purpose of the second series of measurements was to present an example of temporal variation of the ^{222}Rn activity concentration and air electric conductivity in non-stationary conditions dominated by the ^{222}Rn outflow from the tunnel walls and air exchange inside the tunnel. The main findings are summarized in section 7; conclusions are given in section 8.

2. Instrumentation

2.1. Electric Conductivity Sensors

The design of the studied conductivity sensors is based on the time relaxation method, which comprises two steps, i.e., (i) sending a quick voltage perturbation at the electrode level and (ii) measuring the characteristic time of the potential relaxation to the initial unperturbed level. Both sensors (CS-1 and CS-2) consist of the same cylindrical electrodes. Each electrode is connected to a preamplifier with a coaxial bootstrapped cable. The difference between them is the external grid frame, which shelters conductivity sensor-2. The purpose of this grid, which is connected to 0 V, is twofold: (i) to let the gas access inside the grid structure and (ii) to shield the CS-2 electrode from the external electric field. The advantage of this new design with respect to that of the CS-1 sensor (simple electrode without shielding) is that it allows to perform the measurements of the air electric conductivity independently of the external electric field and its variations.

A simplified schematic of the conductivity sensor-2 electrical configuration is shown in Figure 1. The effective coupling of the electrode to the atmosphere is represented by its resistance (R_2), the electrode - grid capacitance by C_2 and the preamplifier by its input capacitance (C_1) and its input resistance (R_1). At the initial phase of a time relaxation sequence, a positive or negative voltage (φ_0) is sent at the preamplifier input through a capacitance (C_0). In the configuration depicted in Figure 1, the temporal variation of the measured potential ($\varphi_1(t)$) is deduced to be as follows:

$$\varphi_1(t) = \varphi_0 \frac{C_0}{C} e^{-t/(RC)}, \quad (1)$$

with $C=C_0+C_1+C_2$ and $R = R_1R_2/(R_1 + R_2)$.

A simplified schematic of the conductivity sensor-1 electrical configuration would be identical to that of CS-2; the only difference is that the term C_2 stands for the electrode capacitance C_{el}.

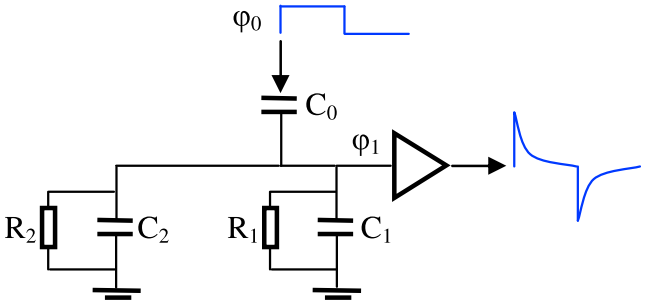

Figure 1. A simplified schematic of the conductivity sensor relaxation measurements.

Equation (1) clearly demonstrates the importance to use a preamplifier with high input resistance for the time relaxation measurements. Otherwise, if $R_1 < R_2$, the relaxation time is simply determined by the input resistance (R_1) of the preamplifier and the measurements turn out to be meaningless. In our design, the input resistance of the preamplifier is measured to be higher than few $10^{15}\Omega$ [*Seran et al.*, 2013]. This is significantly higher than the expected values of the coupling resistance R_2. Thus, $R \approx R_2$ and the characteristic relaxation time is determined by this coupling resistance and the total capacitance of the sensor and its preamplifier.

The coupling resistance R_2 introduced in the simplified schematic of Figure 1 is a parameter that depends not only on the electric conductivity of the gas (σ), but also on the measurement method and on the instrument geometry. Thus, the relationship between the coupling resistance and the air electric conductivity needs to be discussed and evaluated. According to Ohm's law, the resistance is used in relationship between the electric current (I) and the electric potential difference ($\Delta\varphi$), i.e., $I = \Delta\varphi / R_2$, while the electric conductivity is used in relationship between the electric current density (j) and the electric field (E), i.e., $j = \sigma E$. Here the resistance is given in Ω, while the electric conductivity in $\mathrm{S\,m^{-1}}$. Assuming that the electric field around the electrode is mainly determined by the electric charge density on the electrode surface, q_s, and that $E = q_s/\varepsilon_0$, the relationship between the air electric conductivity and the coupling resistance reads as

$$\sigma = \frac{\varepsilon_0}{C_{el} R_2}, \tag{2}$$

where ε_0 is the permittivity of vacuum.

The method described above is used henceforth (i) to estimate the coupling resistance from the fit with the exponential law (1) followed by the sensor measurements during relaxation periods and then (ii) to deduce the gas electric conductivity using (2). The results of the conductivity sensors measurements in different gases, with various atmospheric pressures and different ionization rates controlled by the ^{222}Rn activity concentrations, are presented and discussed in sections 5 and 6. The advantage of the CS-2 design with respect to that of CS-1 is demonstrated in section 6.2.

2.2. ^{222}Rn Activity Concentration Instruments

The AlphaGUARD is a commercial alpha spectrometer from Saphymo. It was operated simultaneously with the conductivity sensors, both in the Roselend tunnel and in the BACCARA chamber. This equipment provides an estimation of ^{222}Rn activity concentration produced by the ^{222}Rn and its progeny decays in air. The AlphaGUARD spectrometer works at the atmospheric pressure above ~800 mbar. It has a minimal temporal resolution of few tens of minutes and measures ^{222}Rn activity concentration in the range from ~few $\mathrm{Bq\,m^{-3}}$ to few $\mathrm{MBq\,m^{-3}}$. Three other sensors that record the pressure of air, its temperature, and relative humidity are integrated in the AlphaGUARD equipment.

The RAD7 is a commercial device from DURRIDGE measuring the activity concentration of radon and thoron in gas. It was used in BACCARA to measure the activity concentration at the end of first low-pressure experiment.

A scintillation flask [*Lucas*, 1957] with a photomultiplier was also used to measure ^{222}Rn activity concentration in BACCARA at the end of the second low-pressure experiment.

All measurements of ^{222}Rn activity concentration in BACCARA are traceable to a primary radon gas standard.

3. ^{222}Rn-Rich Environments

Measurements were carried out in two ^{222}Rn-rich environments presented below.

3.1. Underground Tunnel From the Roselend Natural Laboratory

The Roselend Natural Laboratory is designed and equipped to study the transfer mechanisms of gas and water through the rocks [*Pili et al*., 2004]. Situated in the French Alps close to an artificial lake, it hosts an underground tunnel considered as a key part of the laboratory. This instrumented dead-end tunnel is 128 m long and ~2.4 m in diameter. It lies 7 m below ground surface at the entrance and 55 m at its closed end. It is entirely hosted in crystalline rocks (granite, gneiss, and micaschists). ^{222}Rn gas naturally exhales from the surrounding rocks and accumulates with its progeny in the semiconfined space of the underground tunnel [*Perrier et al*., 2005; *Richon et al*., 2005]. The mean yearly temperature in the tunnel is +8.5°C and the relative humidity is close to 100%. In addition to an observed background ^{222}Rn activity concentration ranging from 200 Bq m^{-3} near the entrance to about 1000 Bq m^{-3} in the most confined section of the tunnel, radon bursts are repeatedly observed with amplitudes reaching up to 80 kBq m^{-3} and durations varying from one to several weeks [*Trique et al*., 1999]. This is due to transient increases in connectivity between the rock matrix and fractures leading to the tunnel and the subsequent radioactive decay and natural ventilation through the tunnel door [*Pili et al*., 2004; *Perrier et al*., 2005; *Richon et al*., 2005]. Environmental parameters, like the atmospheric pressure, air humidity, temperature, O_2, CO_2, and ^{222}Rn activity concentrations, are permanently surveyed with sensors installed in the tunnel.

During short campaigns in September and October 2015, the conductivity sensors were placed in a side room situated at mid-distance along the tunnel and referred to as the inner room. A metal door allows for some isolation of the inner room from the main tunnel. The total volume and the surface area of the inner room are ~496 m^3 and ~1250 m^2, respectively [*Perrier et al*., 2005].

3.2. BACCARA Radon Chamber

BACCARA is a test bench developed to study ^{222}Rn and its progeny decay and used for calibration ^{222}Rn measuring instruments. This facility gives a possibility to establish the ^{222}Rn activity concentration in range from ~40 Bq m^{-3} to ~40 kBq m^{-3} (and even more if needed) and with various environmental conditions [*Michielsen and Voisin*, 1999]. For example, it allows to simulate the 6 mbar Martian atmosphere composed with CO_2 gas. The BACCARA installation is equipped with different ^{222}Rn sources and ^{222}Rn activity concentration instruments, the measurements of which are traceable to a primary radon source [*Picolo et al*., 2000]. The generated ^{222}Rn activity concentration is either quasi-stationary or naturally decreasing (with a half-life of ~3.8 days). The BACCARA chamber is also equipped with (i) a vacuum pump that permits to create a partial vacuum down to ~ mbar pressure, (ii) a gas injection system that allows a steady insertion of different gases, and (iii) several sensors to control the pressure, temperature, and relative humidity. The chamber represents a hermetic, electrically grounded, stainless steel cylinder with a diameter of 1 m and a length of ~1.3 m.

4. From ^{222}Rn Activity Concentration to the Air Electric Conductivity

An analytical model is proposed in this section with intention to explain the measured values of the air electric conductivity at different ^{222}Rn activity concentrations and to estimate the effect of the loss of alpha particles and ions on the chamber walls at different atmospheric pressures.

4.1. From ^{222}Rn Activity Concentration to Ion Production Rate

Radon-222 decays to its progeny (^{218}Po, followed by the 214 and 210 isotopes of Pb, Bi, and Po until stable ^{206}Pb). This decay chain is associated with emissions of alpha ($^4He^{++}$) or beta (e^-) particles. Because of their size and energy, the alpha particles are considered as a major source of air ionization. During its motion in a gas, each alpha particle undergoes numerous collisions with neutral species (molecules and atoms). These collisions result in a loss of energy of the alpha particles and in the generation of ions of both polarities. The total number of ions produced by each alpha particle along its trajectory is thus determined by the ratio of alpha's initial energy, E^0_α, to the gas ionization energy, E_i. The ion production rate, β, is then estimated as a product of the activity concentration, B_k, of four alpha emitters (^{222}Rn, ^{218}Po, ^{214}Po and ^{210}Po) and the number of ions generated during each alpha's path. It reads as

$$\beta = \sum_{k=1}^{n_a} B_k E^0_{\alpha k} / E_{ik}, \tag{3}$$

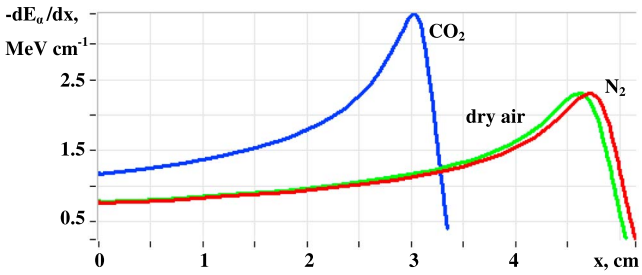

Figure 2. Energy loss rate of 6 MeV-alpha particle versus distance along its path in dry air (green line), nitrogen (red line), and carbon dioxide (blue line) at P=975 mbar and T=25°C.

where n_α=4; $E_{ik}\approx$35 eV in air and CO_2 [*Jess and Sadaukis*, 1957; *Price*, 1964], and the initial alpha energies equal to $E^0_{\alpha1}\approx$5.6 MeV, $E^0_{\alpha2}\approx$6 MeV, $E^0_{\alpha3}\approx$7.8 MeV and $E^0_{\alpha4}\approx$5.3 MeV for ^{222}Rn, ^{218}Po, ^{214}Po and ^{210}Po, respectively [*Bé et al.*, 2013]. In an open space, ^{222}Rn and its short-lived progeny (i.e., ^{218}Po and ^{214}Po) are not in equilibrium. But in a closed volume, like BACCARA, this equilibrium is reached due to deposition of ^{222}Rn solid progeny onto the chamber walls. The contribution of the ^{210}Po alpha emitter is negligible because of the long life of this progeny. The ^{222}Rn solid progeny are rapidly attached to the nearby solid surfaces, and thus, only half of the alpha particles is assumed to contribute to air ionization. Taking into account these considerations, equation (3) reads as

$$\beta = B\cdot\sum_{k=1}^{n_\alpha}\gamma_k E^0_{\alpha k}/E_{ik}, \tag{4}$$

where n_α=3, B=B_1, γ_1=1 for ^{222}Rn and γ_2=γ_3=0.5 for ^{218}Po and ^{214}Po. Applying this formula for a ^{222}Rn activity concentration of 1 kBq m^{-3} gives $\beta\approx3.6\cdot10^8$ m^{-3} s^{-1}.

The rate of the energy loss, $-\mathrm{d}E_\alpha/\mathrm{d}x$, is not constant along the alpha trajectory but gradually increases following Bragg's law [see, e.g., *Bethe*, 1930; *Price*, 1964; *International Commission on Radiation Units and Measurements (ICRU)*, 1993]. The distance traveled by an alpha particle in a gas depends not only on its initial energy and the ionization energy but also on the gas atomic composition and its concentration. Examples of the alpha energy loss rate variation with distance are displayed for different gases in Figure 2, as given in the ASTAR database [*ICRU*, 1993]. At an atmospheric pressure of 975 mbar, the distance traveled by a 6 MeV alpha particle until being stopped is around 5 cm in dry air (green line) or N_2 (red line) and is around 3.3 cm in CO_2 (blue line). According to Figure 2, the alpha particles loose around 30% of their energies in the last quarter of their trajectory.

The distance traveled by alpha particles in gas increases when the gas pressure decreases. At 6 mbar, the path of 6 MeV alpha particles is expected to be around 8.4 m in N_2 and around 5.4 m in CO_2. Such long paths for alpha particles might result in a significant decrease of the ionization rate in case of ^{222}Rn decay in an enclosed space. Once it collides with a solid structure, the alpha particle looses the rest of its energy within a thin layer of few microns of this structure. An example of the probability distribution of the alpha particle path length calculated for the dimensions of the BACCARA chamber and at a pressure of ~6 mbar is shown in Figure 3. The mean path length of 6 MeV alpha particles is thus estimated to be ~0.86 m. Integrating $-\mathrm{d}E_\alpha/\mathrm{d}x$ over the alpha particle path, we conclude that only ~14% of the initial energy of the alpha particle will contribute to ionization in CO_2 and twice less (~7%) in N_2 at 6 mbar in the BACCARA chamber.

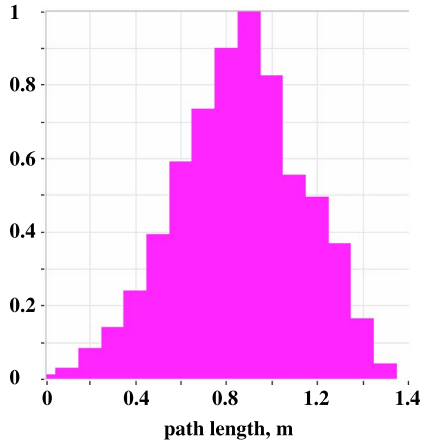

Figure 3. Probability distribution of 6 MeV-alpha path length in the BACCARA chamber (cylinder with a diameter of 1 m and a length of 1.3 m) at 6 mbar pressure. Mean value is estimated to be ~0.86 m.

4.2. From Ion Production Rate to Ion Concentration

Some part of the newly created ions is lost. In addition to the ion-ion recombination, an outflow of ions at the chamber walls might become an essential

sink of ions. In the case of an enclosed space, the ion balance equation can be written as follows:

$$\frac{dn_i}{dt} = \beta - \alpha n_i^2 - \kappa n_i, \tag{5}$$

where n_i is the ion density, which is assumed hereafter to be the same for positive and negative ions; t is the time; β is the ion production rate (introduced in section 4.1); α (in $m^3 s^{-1}$) is the ion recombination coefficient; and κ (in s^{-1}) is the ion outflow frequency at the chamber walls. In absence of electric charging, the outflow frequency of light ions at the chamber walls is mostly defined by the Brownian diffusion [see, e.g., *Park et al.*, 2001]. Otherwise, this coefficient is determined by the average electric field inside the chamber E and reads as $\kappa \approx \mu ES/V$. Here μ is the ion mobility (in $m^2 s^{-1} V^{-1}$), S and V are the walls surface area and the chamber volume, respectively. Brownian diffusion process depends essentially on the gas temperature and the gas viscosity, while the ion diffusion in an electric field depends on the ion mobility and, thus, on the gas pressure. Measurements performed in the BACCARA chamber and presented in section 5 clearly demonstrate a correlation between the ion outflow frequency at the chamber walls and the gas pressure. Thus, Brownian diffusion to the wall is omitted in equation (5).

In stationary conditions, when $dn_i/dt = 0$, the equation (5) has the following solution:

$$n_i = \frac{-\kappa/2 + \sqrt{(\kappa/2)^2 + \alpha\beta}}{\alpha}. \tag{6}$$

When the ion sink at walls is insignificant, the above solution tends to the solution in an open space and simply reads as:

$$n_i = \sqrt{\beta/\alpha}. \tag{7}$$

4.3. From Ion Concentration to Air Electric Conductivity

The electric conductivity of air, σ, is a parameter which characterizes the capacity of light ions to carry the electric current in the atmosphere. This parameter is determined by the ion density, the ion mobility and the electric charge of each ion, q. It is expressed in $S m^{-1}$ and is estimated as

$$\sigma = q\mu n_i. \tag{8}$$

5. Measurements in the BACCARA Chamber

5.1. Tests Description

A few-day observational campaign was carried out in the IRSN BACCARA facility in June 2016. The purpose was to measure the air electric conductivity with two conductivity sensors (CS-1 and CS-2) in quasi-stationary conditions at different levels of the ^{222}Rn activity concentration and gas atmospheric pressure. The accommodation of the conductivity sensors and other equipments inside and outside the BACCARA chamber are seen in the photo of Figure 4. Three series of measurements, performed in BACCARA, are presented and discussed in the sections 5.2 and 5.3.

At first, the ^{222}Rn activity concentration was set to ~1 kBq m^{-3} and then increased step by step to ~8 kBq m^{-3}. These tests were carried out with a permanent injection of dry air through a ^{222}Rn source, balanced with a controlled air evacuation to set up a constant atmospheric pressure of 975 mbar. The dry air speed, typically ranging from ~1 to 8 m s^{-1}, was fixed during each sequence and provided the desired level of the ^{222}Rn activity concentration in the chamber. A portable fan (see Figure 4) ensured a regular mixing of the newly injected gas with the air of the chamber. Quasi-stationary conditions of the ^{222}Rn activity concentration inside BACCARA were reached in ~2 h, but the equilibrium of ^{222}Rn progeny activity concentration was typically attained in ~3 h after the beginning of each sequence. The ^{222}Rn activity concentration was measured continuously with an AlphaGUARD (described in the section 2.2), installed inside the chamber and seen in Figure 4.

Afterward, the AlphaGUARD was removed from the BACCARA, and the vacuum pump was used to decrease the atmospheric pressure down to ~1 mbar. Then, several injections of CO_2 followed by depressurization were performed in order to obtain a pure CO_2 atmosphere at 1 mbar inside the chamber. The ^{222}Rn activity concentration was fixed at 14.9 kBq m^{-3}, while the atmospheric pressure was increased step by step from ~1

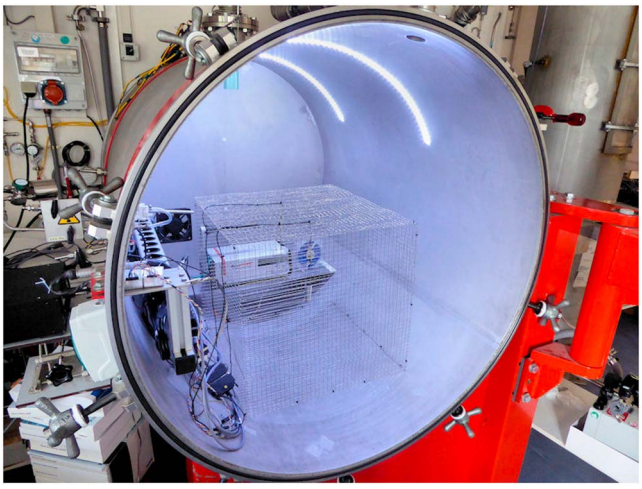

Figure 4. Setting of the conductivity sensors tests in the BACCARA chamber.

to 975 mbar. Typically, the gas was reinjected in the BACCARA chamber periodically, i.e., each 30–40 min, to set up the predetermined gas pressures. CO_2 was injected to set up the pressures below 100 mbar, while dry air was used to set up the pressures above 100 mbar. The volume activity during these tests was considered to be stable for the temporal intervals (typically few hours) significantly shorter than the ^{222}Rn half-life (~3.82 days). The ^{222}Rn activity concentration at the time of the electric conductivity measurements was estimated from the ^{222}Rn activity concentration measured at the end of the tests with a RAD7 placed outside the BACCARA (by analyzing the gas sample) and taking into account the time that passed between our tests and these measurements.

A similar sequence was repeated for a slightly higher ^{222}Rn activity concentration, i.e., of 18–21 kBq m^{-3}, generated with a different radioactive source and using only CO_2 gas to establish the predetermined pressure levels. A scintillation flask and a photomultiplier were used to measure the ^{222}Rn activity concentration at the end of the test.

5.2. Electric Conductivity of Air Versus ^{222}Rn Activity Concentration

The purpose of the first sequence of measurements in the BACCARA chamber was (i) to figure out the relationship between the ^{222}Rn activity concentration, ion density, and electric conductivity of air at quasi-stationary volume radioactivity and (ii) to estimate the impact of the ion sink on the chamber walls and internal structures. The tests were carried out at an atmospheric pressure of 975 mbar and with dry air. Four levels of the ^{222}Rn activity concentration were generated, i.e., 1, 2.3, 3.8, and 7.8 kBq m^{-3}. The electric conductivity of air was measured 3 h after the beginning of each observational sequence. The values of the air electric conductivity deduced from the time relaxation measurements performed with the conductivity sensor-1 and conductivity sensor-2 (for details see section 2.1) are shown in Figure 5, where the analytical

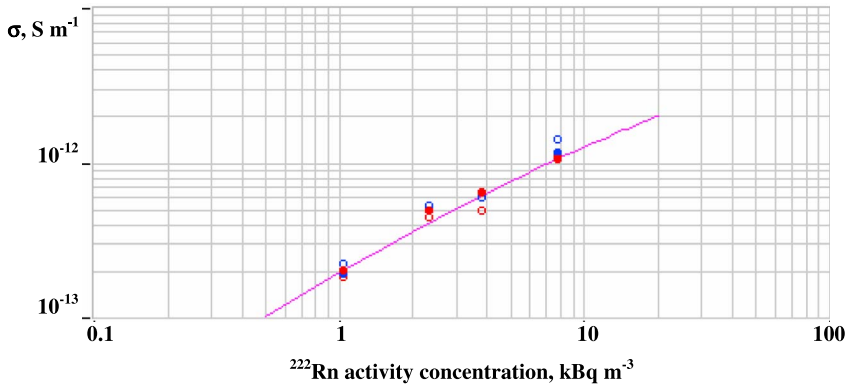

Figure 5. Electric conductivity of dry air measured by the conductivity sensors in the BACCARA chamber at different levels of the ^{222}Rn activity concentrations, i.e., 1, 2.3, 3.8, and 7.8 kBq m^{-3}. The atmospheric pressure inside the chamber was maintained at 975 mbar and the air relative humidity at ~5%. Red and blue circles indicate electric conductivity carried by the positive and negative ions, respectively. Filled and empty circles correspond to the measurements of the conductivity sensor-1 and conductivity sensor-2, respectively. Mauve line shows the analytical solution (8) for the air electric conductivity with the ion density and the ion production rate calculated using equations (6) and (4), respectively. Parameters used to calculate the best fit of the measured points are the following: $\alpha = 1.6 \cdot 10^{-12}$ m^3 s^{-1}, $\mu = 2.6 \cdot 10^{-4}$ m^2 V^{-1} s^{-1}, and $\kappa = 250\mu$ s^{-1}.

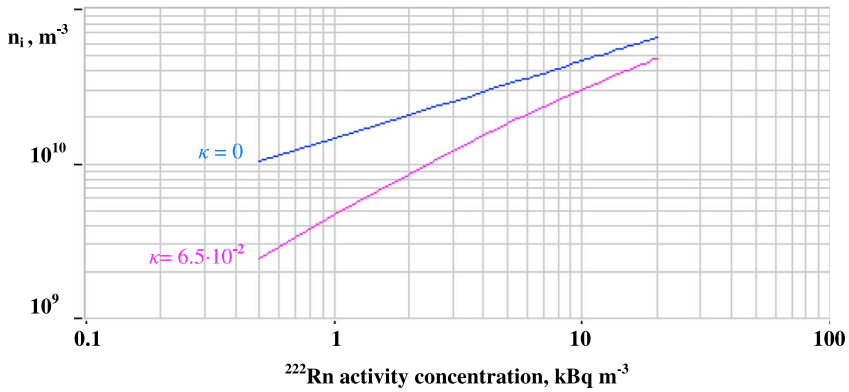

Figure 6. (mauve line) Ion density which corresponds to the air electric conductivity shown by mauve line in Figure 5. (blue line) Ion density calculated using the same parameters as for the mauve line but with the assumption that there is no ion sink on the chamber walls; i.e.,κ=0.

solutions (8) for the air electric conductivity with the ion density and ion production rate calculated using the equations (6) and (4), respectively, are also reported. Parameters that allow getting the best fit of the measured points are the following: ion recombination coefficient α=1.6·10^{-12}m^{-3}s^{-1}, ion mobility μ=2.6·10^{-4}m^{2}V^{-1}s^{-1} and ion outflow frequency at the chamber walls κ=250μs^{-1}. The ion recombination coefficient and ion mobility are estimated to be in accordance with the values reported in literature [see, e.g., *Shreve*, 1970; *Hõrrak et al*., 2000; *Harrison and Tammet*, 2008].

In order to estimate the contribution of the ion sink on the chamber walls into the ion balance established inside the chamber, two solutions are displayed in Figure 6. First, the ion density is calculated using equation (6) with the parameters that were previously found to fit the measured values of the air electric conductivity. Second, the ion density is calculated assuming that the ion sink on the chamber walls and its internal structures is negligible, i.e., κ=0. A noticeable difference between the two solutions, i.e.,factor of ~3.6 at 1 kBq m^{-3} and ~1.8 at 7.8 kBq m^{-3}, demonstrates that the ion outflow on the chamber walls was essential in the conditions at which the tests were carried out. Potential reason of this phenomenon is the electric charging of different insulators found inside the chamber (electrical socket, cables, wood plate, plastic ventilator, etc.), which is likely amplified by the air motion produced by the gas injection and ventilation systems settled in the chamber. The surface electric charges generate the electric field that controls the ion motion and their subsequent loss on the chamber walls, its internal structures and equipments. In the example considered in this section (Figures 5 and 6), the average electric field is estimated to be ~40 V m^{-1}.

5.3. Electric Conductivity Versus Gas Pressure

The purpose of the second sequence of measurements in the BACCARA chamber was to look for the relationship between the gas pressure and gas electric conductivity in the conditions of a fixed ^{222}Rn activity concentration. Few pressure steps were chosen to perform the measurements; 6, 20, and 100 mbar were attained with injection of CO_2, then 200 and 975 mbar were attained with injection of dry air. The ^{222}Rn activity concentration was estimated to be ~14.9 kBq m^{-3} during the whole observational period of few hours.

The electric conductivity of the injected gas deduced from the time relaxation measurements performed with the conductivity sensor-1 is shown in Figure 7. The analytical solutions (8) for the electric conductivity of CO_2 and dry air with the ion density and ion production rate calculated using equations (6) and (4), respectively, are displayed in the same figure. The best fit of the measured values in CO_2 gas, as well as in dry air, is also reported. Parameters used to obtain these fits are the following: κ=5μs^{-1}, α=1.6·10^{-12}m^{-3}s^{-1} in dry air and α=0.8·10^{-12} m^{-3} s^{-1} in CO_2. The ion mobility μ is assumed to vary inversely as the gas pressure P:

$$\mu(P) = \mu_0 P_0 / P, \tag{9}$$

where P_0=975 mbar, μ_0=3.6·10^{-4}m^{2}V^{-1}s^{-1} in dry air, and μ_0=1.6·10^{-4}m^{2}V^{-1}s^{-1} in CO_2.

Two other solutions were appended in Figure 7 with the aim to illustrate the effect of the loss of alpha particles and ions on the chamber walls. One corresponds to the electric conductivity variation versus CO_2 gas pressure,

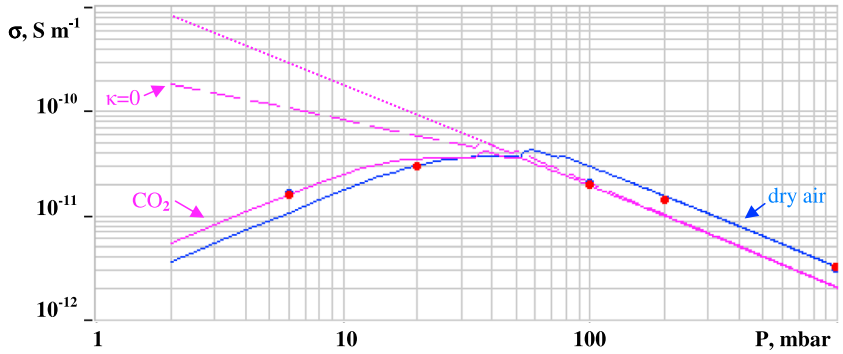

Figure 7. Electric conductivity of gas (σ) measured by the conductivity sensor-1 in the BACCARA chamber at a fixed ^{222}Rn activity concentration of 14.9 kBq m^{-3} and at different gas pressures (P). CO_2 was injected in the chamber to set up the low-pressure levels, i.e., 6, 20, and 100 mbar. Higher pressures, i.e., 200 and 975 mbar, were attained with dry air injection. Red and blue filled circles indicate the electric conductivity carried by the positive and negative ions, respectively. Solid lines show the analytical solutions (8) for the electric conductivity of CO_2 (mauve) and dry air (blue) with the ion density, ion mobility, and ion production rate calculated using equations (6), (9), and (4), respectively. Parameters used to obtain the best fits of the measured points are the follows: $\alpha = 1.6 \cdot 10^{-12}$ m^{-3} s^{-1}, and $\kappa = 5\mu$s^{-1}, with $\mu_0 = 3.6 \cdot 10^{-4}$ m^{2}V^{-1} s^{-1} in dry air, and $\alpha = 0.8 \cdot 10^{-12}$ m^{-3} s^{-1}, and $\kappa = 5\mu$s^{-1} with $\mu_0 = 1.6 \cdot 10^{-4}$ m^{2}V^{-1} s^{-1} in CO_2. Mauve dashed line stands for the electric conductivity variation versus pressure in the CO_2 gas assuming that there are no sink of ions on the chamber walls. Mauve dotted line displays the electric conductivity assuming no loss of alpha particles on the chamber walls.

which is calculated assuming that there is no sink of ions on the chamber walls. The other represents the electric conductivity of CO_2 gas found in the same conditions as the first one but assuming that there is no loss of alpha particles on the chamber walls (case of an open space or a very big chamber). At a gas pressure below ~60 mbar in dry air and below ~40 mbar in CO_2, the mean alpha particle path length in the BACCARA chamber is estimated to be about 0.86 m (section 4.1). Once the path length of alpha particles exceeds this value, the particle is lost on the walls before the end of its free path in the gas. This loss reduces the ionization rate inside the chamber. The rate of the ion loss on the internal surfaces of the chamber (walls, internal structures, and equipment) depends on the electric charging of these structures and also on the ion mobility. The later is determined by the mass of light ions (and thus by the type of gas) and varies inversely with the gas pressure, following (9). The combination of both phenomena, i.e., loss of alpha particles and sink of ions, produces an essential decrease of the ion density in the chamber enclosure at lower gas pressure. At 6 mbar and in a CO_2 atmosphere, for example, the ion density is reduced by a factor of ~20 with respect to its magnitude at 975 mbar. The ion density, calculated from the gas electric conductivity (shown in Figure 7) and applying (8) and (9), is presented in Figure 8. The steps on the curves of the electric conductivity and ion density versus gas pressure around 60 mbar in dry air and ~40 mbar in CO_2 are due to the fact that in our analytical model the alpha particle is lost on the walls once its path length exceeds 0.86 m. Thus, the probability distribution of alpha path length (shown in Figure 3) was replaced for simplicity reasons by its mean value.

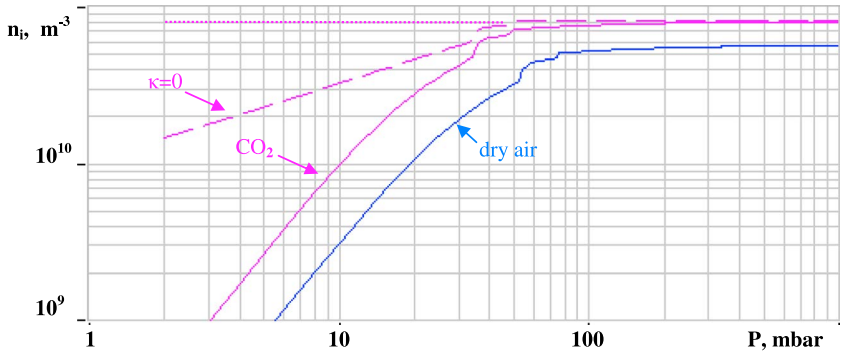

Figure 8. Ion density (n_i) versus gas pressure (P) deduced from the electric conductivity represented in Figure 7. Descriptions of different types of lines and their colors are identical to those of Figure 7.

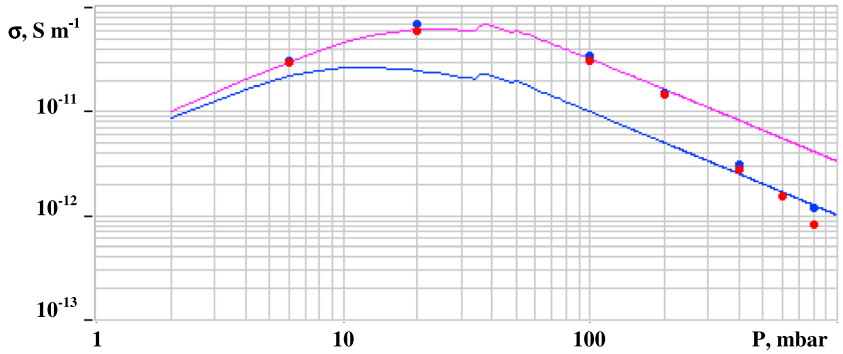

Figure 9. Electric conductivity (σ) of gas deduced from the conductivity sensor-1 measurements (solid circles) in the BACCARA chamber at a fixed ^{222}Rn activity concentration and at different gas pressures (P). CO_2 was reinjected in the BACCARA chamber each 30–40 min to set up the predetermined gas pressures, i.e., 6, 20, 100, and 200 mbar on the first day and 400, 600, and 800 mbar on the second day (18 h later). ^{222}Rn activity concentration was measured to be 21 kBq m^{-3} on the first day and 18 kBq m^{-3} on the second day. Solid lines show the analytical solutions (8) for the electric conductivity of the CO_2 gas with the ion density, ion mobility, and ion production rate calculated using equations (6), (9), and (4), respectively. Mauve and blue lines display the best fit of the measurements on the first and on the second day, respectively. Parameters used to obtain these fits are the following: $\alpha = 0.8 \cdot 10^{-12}$ m^{-3} s^{-1}, $\kappa = 3.8 \mu$s^{-1}, and $\mu_0 = 2.2 \cdot 10^{-4}$ m^2 V^{-1} s^{-1} and $\alpha = 1.6 \cdot 10^{-12}$ m^{-3} s^{-1}, $\kappa = 3.8 \mu$s^{-1}, $\mu_0 = 10^{-4}$ m^2 V^{-1} s^{-1} for the first and the second day series, respectively.

The third sequence of measurements, rather similar to the second one, was conducted at slightly higher ^{222}Rn activity concentration, i.e., of 18–21 kBq m^{-3}, and using only CO_2 gas injections to get the stipulated gas pressure. In contrast with the previous series, the tests were carried out over 2 days. The measurements at 6, 20, 100, and 200 mbar were performed during the afternoon of the first day, while the observations at 400, 600, and 800 mbar were concluded in the morning the following day. ^{222}Rn activity concentration was measured to be 21 kBq m^{-3} on the first day and 18 kBq m^{-3} on the second day. The objective of the third sequence was to confirm the results obtained during the tests at 14.9 kBq m^{-3} and to compare the parameters deduced from the time relaxation measurements made with the two conductivity sensors CS-1 and CS-2.

By analogy with the results presented in Figures 7 and 8, Figures 9 and 10 display, respectively, the electric conductivity and ion density calculated from the coupling resistances measured by the conductivity sensors. In the same figure the analytical solution (8) for the electric conductivity of CO_2 gas with the ion density, ion mobility, and ion production rate calculated using equations (6), (9), and (4), respectively, is displayed. In Figure 9 the best fits of the electric conductivity values deduced from the CS-1 measurements during the first day and during the second day are presented. Parameters used to obtain these fits are estimated as follows:

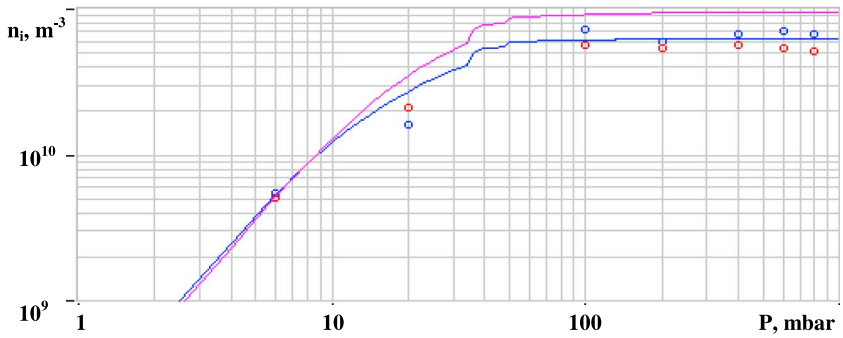

Figure 10. Ion density (n_i) versus gas pressure (P) deduced from the conductivity sensor-1 and conductivity sensor-2 measurements. The mauve line corresponds to the mauve line shown in Figure 9 and displays the best fit of the measurements with conductivity sensor-1. Red and blue circles indicate the positive and negative ion density, respectively, deduced from the conductivity sensor-2 measurements. Blue line shows the analytical solution (6) for the ion density with the ion mobility and ion production rate calculated using equations (9) and (4), respectively. Parameters used to get the best fit of the displayed points are the following: $\alpha = 1.6 \cdot 10^{-12}$ m^{-3} s^{-1}, $\kappa = 6.5 \mu$s^{-1}, and $\mu_0 = 10^{-4}$ m^2 V^{-1} s^{-1}.

Figure 11. Conductivity sensors tests in the inner room of the Roselend tunnel. The metal door used to isolate the inner room from the tunnel is open half-way. The Sensor is set in the middle of the inner room. The operator is sitting outside the inner room, in the tunnel. Surfaces appear shinny due to moisture condensation.

$\alpha=0.8\cdot10^{-12}m^{-3}s^{-1}$, $\kappa=3.8\mu s^{-1}$ and $\mu_0=2.2\cdot10^{-4}m^2V^{-1}s^{-1}$ and $\alpha=1.6\cdot10^{-12}m^{-3}s^{-1}$, $\kappa=3.8\mu s^{-1}$, and $\mu_0=10^{-4}\ m^2\ V^{-1}\ s^{-1}$ for the first and second day series, respectively. The decrease of the electric conductivity observed during the second day with respect to the theoretically expected values is possibly due to the outgassing of different structures inside the chamber (electrical socket, cables, and wood plate). These gas impurities might result in an increase of the mass of ions and their effective diameters and thus produce a decrease of the ion mobility [see, e.g., *Cabane et al.*, 1976]. Such phenomenon was not observed during the second sequence of measurements, which was much shorter (few hours).

The parameters found to fit the electric conductivity measured by the conductivity sensor-1 during the first day are then applied to calculate the ion density (Figure 10). As previously done, the relationship between the ion density, the electric conductivity, the ion mobility, and the gas pressure was used following equations (8) and (9) to deduce the magnitudes of the ion density from the measurements of the conductivity sensor-2. With respect to CS-1, the coupling resistance deduced from CS-2 in the ^{222}Rn-rich gas is directly proportional to the ion density and does not vary with the ion mobility. The analytical solution (6) for the ion density with the ion mobility and the ion production rate calculated using equations (9) and (4), respectively, is shown in Figure 10. The best fit of the displayed data points is found with $\alpha=1.6\cdot10^{-12}$ $m^{-3}s^{-1}$, $\kappa=6.5\mu s^{-1}$, and $\mu_0=10^{-4}m^2V^{-1}s^{-1}$. A higher rate of the ion sink, as found to best fit the CS-2 measurements with respect to that estimated from the CS-1 data, is likely explained by an additional ion sink at the grid frame that envelopes the CS-2 electrode. Detailed modeling of the responses of the conductivity sensors in different environmental conditions and with different types of ionization sources is beyond the scope of this paper.

6. Measurements in the Roselend Tunnel

6.1. Tests Description

Natural environmental conditions found in the Roselend tunnel (Figure 11) are very different to those created in the BACCARA chamber. The tunnel's air was cold and extremely moist. The measured relative humidity fluctuated around 97%. The temperature was rather constant at +8.5°C, while the atmospheric pressure measured during the experiments was ~845 mbar. To make instruments work properly in such environment is not a simple task: condensation of water at sensible parts of sensors may perturb the measurements done and even lead to short circuit. Thus, particular precautions are needed to get meaningful observations.

Two sequences of measurements of the air electric conductivity performed in the inner room (for details see section 3.1) of the Roselend tunnel are presented in the following sections 6.2 and 6.3. The objective of the first test was to demonstrate the functioning and performances of the two types of conductivity sensors, CS-1

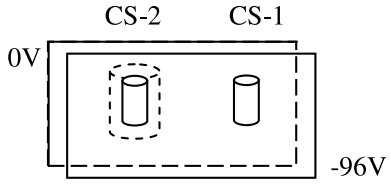

Figure 12. A simplified schematic of the CS-1 and CS-2 mounted between two polarized aluminum sheets during tests conducted in the Roselend tunnel.

and CS-2, in an external electric field. The purpose of the second sequence was to examine the relationship between the ^{222}Rn activity concentration and the air electric conductivity measured inside the inner room and to figure out the influence on these parameters of the air exchange between the inner room and the tunnel as well as the ^{222}Rn exhalation flux at the walls.

6.2. Conductivity Sensors Measurements in an External Electric Field

In this test, the two conductivity sensors CS-1 and CS-2 were implemented between two parallel aluminum sheets, which were grounded at the beginning of the observation sequence. Few tens of minutes later, one of the sheets was polarized negatively at −96V, while the other stayed at 0V. The two sensors were mounted symmetrically and at an equal distance of ~7.5 cm from both sheets and measured simultaneously. Such configuration (schematically represented in Figure 12) permits to create an external electric field identical for both sensors and equals to 0 V m^{-1} and 430 V m^{-1}, respectively, at the beginning of the test and after the polarization of the sheets. The time relaxation measurements performed with the two conductivity sensors are shown in Figure 13. The electric conductivity of air during this test is estimated to be ~$1.1 \cdot 10^{-12}$ S m^{-1}, while the ^{222}Rn activity concentration was measured to be ~2 kBq m^{-3}. As presented in Figure 13, the time relaxation measurements of the CS-2 sensor sheltered inside the 0V−grid frame are not perturbed by the applied external field. The only change is a shift of the CS-2 continuous potential from −0.5V to −0.6V. This shift is due to the CS-2 frame efficiency, which is directly related to the grid transparency, the sensor geometry, and the field direction. In contrast with the CS-2 results, the time relaxation measurements performed in the external field of 430 V m^{-1} with the CS-1 sensor (Figure 13) does not make sense anymore, since the electric field created by the electrode polarization becomes too low with respect to the external DC and AC electric field to control the ion motion.

6.3. Relationship Between the ^{222}Rn Activity Concentration and Air Electric Conductivity

Below, the temporal variations of the ^{222}Rn activity concentration and the electric conductivity of air in the inner room of the Roselend tunnel are discussed.

6.3.1. Temporal Variation of the ^{222}Rn Activity Concentration in the Inner Room of the Roselend Tunnel

Following the approximation of *Wilkening and Watkins* [1976], the temporal variation of the ^{222}Rn activity concentration, *B*, in the air of an enclosure of volume *V* and surface *S* is given by

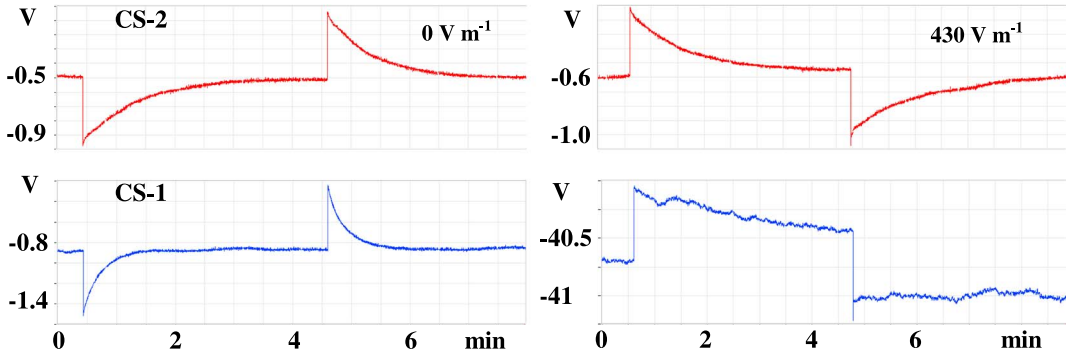

Figure 13. Time relaxation measurements performed with two conductivity sensors, i.e., CS-2 (in red) and CS-1 (in blue), in the inner room of the Roselend tunnel. The external electric field was generated by two polarized parallel aluminum sheets mounted according to the schematic of Figure 12. Left and right columns correspond to the measurements conducted with an electric field of 0 and 430 V m^{-1}, respectively. The electric conductivity of air carried by the negative and positive ions is estimated to be ~$1.2 \cdot 10^{-12}$ and 10^{-12} S m^{-1}, respectively, while the ^{222}Rn activity concentration is measured to be ~2 kBq m^{-3}.

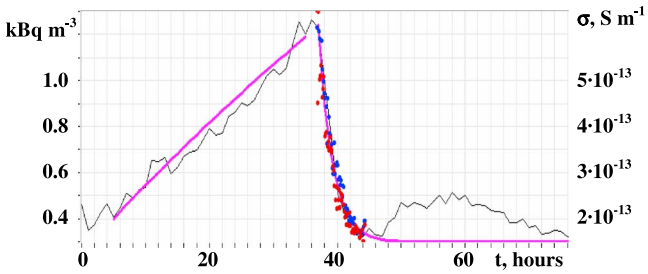

Figure 14. Temporal variation of the ^{222}Rn activity concentration in the inner room of the Roselend tunnel measured with an AlphaGUARD equipment (black line). The door of the inner room was closed at the beginning of the displayed period and was opened 37 h later. Mauve line shows the temporal variation of the ^{222}Rn activity concentration calculated using equation (11) with $\Phi = 3.6 \cdot 10^{-3}$ Bq m^{-2} s^{-1}, $\lambda_v = 0\,s^{-1}$ before 37 h and $\lambda_v = 1.25 \cdot 10^{-4}$ s^{-1}, $B_{ext} = 230\,Bq\,m^{-3}$ after 37 h. The temporal variation of the electric conductivity measured with conductivity sensor-1 is shown with dots. Red and blue dots correspond to the positive and negative electric conductivities, respectively.

$$\frac{dB}{dt} = \frac{S}{V}\Phi - \lambda B - \lambda_v (B - B_{ext}), \tag{10}$$

where Φ is the ^{222}Rn exhalation outflow from the room walls, λ the ^{222}Rn decay constant ($2.1 \cdot 10^{-6}\,s^{-1}$), and λ_v the ventilation rate by air with a ^{222}Rn activity concentration B_{ext}. Equation (10) has the following solution:

$$B(t) = \frac{-\left[\frac{S}{V}\Phi - B_0(\lambda + \lambda_v) + \lambda_v B_{ext}\right] e^{-(\lambda+\lambda_v)t} + \lambda_v B_{ext} + \frac{S}{V}\Phi}{(\lambda + \lambda_v)}, \tag{11}$$

with $B_0 = B(t=0)$. In the condition $(\lambda + \lambda_v)t << 1$, the formula (11) can be simplified and written as

$$B(t) = B_0 + \left[\frac{S}{V}\Phi - B_0(\lambda + \lambda_v) + \lambda_v B_{ext}\right] t. \tag{12}$$

For time periods sufficiently short, i.e., typically about 1 h, the ^{222}Rn activity concentration varies linearly with time. For longer time periods, equation (11) is relevant. For time intervals longer than 20 days and without air exchange, the ^{222}Rn activity concentration tends toward the constant $S\Phi/(V\lambda)$. Equations (11) and (12) are valid when the ^{222}Rn outflow from the room walls and ^{222}Rn activity concentration outside the room are at steady state.

The ^{222}Rn activity concentration was measured during 80 h in the inner room of the Roselend tunnel with a time step of 1 h with an AlphaGUARD equipment. At the beginning of the observational sequence, the door of the inner room was closed in order to strongly diminish the air exchange between the inner room and the tunnel. During the first 35 h the radon activity concentration is observed to increase from ~400 to 1200 Bq m^{-3} with the rate of ~$7.4 \cdot 10^{-3}$ Bq m^{-3} s^{-1}. After the opening of the room door, which took place 37 h later, the ^{222}Rn activity concentration rapidly decreases during 3 h with the rate of ~$6.5 \cdot 10^{-2}$ Bq m^{-3} s^{-1}. Following discussion given earlier in this section, the equation (11) was applied to fit the measured temporal variation of the ^{222}Rn activity concentration. The temporal variation of the ^{222}Rn activity concentration calculated for two periods, i.e., before $t = 37$ h (thus without air exchange) and after $t = 37$ h (with ventilation), are shown in Figure 14. Following the assumption that all parameters stay approximately unchanged during the whole period of observations, the ^{222}Rn exhalation outflow from the room walls, its ventilation rate, and its activity concentration in the tunnel, i.e., outside the inner room, are estimated to be as follows: $\Phi = 3.6 \cdot 10^{-3}$ Bq m^{-2} s^{-1}, $\lambda_v = 1.25 \cdot 10^{-4}\,s^{-1}$ and $B_{ext} = 230\,Bq\,m^{-3}$. If the estimated ^{222}Rn exhalation outflow from the surrounding rocks looks similar to that published by *Perrier et al.* [2005]; the ventilation rate is unsurprisingly found to be much higher (~10^2 times) with respect to the previously published values because of the recent commissioning of a gentle venting system at the tunnel entrance.

6.3.2. Temporal Variation of the Electric Conductivity of Air in the Roselend Tunnel Inner Room

During the second period, i.e., after the opening of the door that separates the inner room from the tunnel, the measurements were carried out simultaneously with the conductivity sensor-1 and the AlphaGUARD. Temporal resolutions of the electric conductivity and ^{222}Rn activity concentration measurements were

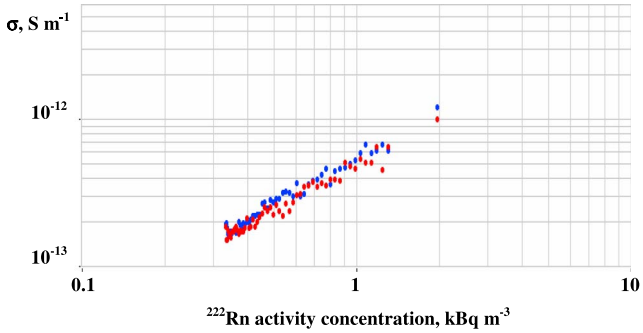

Figure 15. Electric conductivity (σ) of moist air, measured by the conductivity sensors in the inner room of the Roselend tunnel, versus ^{222}Rn activity concentration, at the pressure of 845 mbar and air relative humidity of 97%. Red and blue dots indicate the electric conductivity carried by the positive and negative ions, respectively.

chosen to be 4 min and 1 h, respectively. Variation of the air electric conductivity versus time is presented in Figure 14 with the measured and theoretical ^{222}Rn activity concentrations. The fact that the electric conductivity perfectly follows the ^{222}Rn activity concentration variation demonstrates that (i) the air ionization is controlled by the ^{222}Rn and its progeny and that (ii) in the non-stationary conditions, like those produced by the air exchange between the inner room and the tunnel, the concentration of light ions is merely proportional to the ^{222}Rn activity concentration.

By analogy with the results of the tests performed in dry air of the BACCARA chamber and presented in Figure 5, Figure 15 shows the electric conductivity of air versus ^{222}Rn activity concentration measured in the inner room of the Roselend tunnel. Depicted in this figure are the measurements of the conductivity sensor-1 performed during two observational sequences displayed in Figures 13 and 14. An attempt to compare the results obtained in the Roselend tunnel with those obtained in the BACCARA chamber is inappropriate for few raisons. At first, the ^{222}Rn generation in the BACCARA is controlled, and the measurements were performed in the quasi-stationary conditions, in contrast with the observations made in the Roselend tunnel. Second, the small volume inside structures that contain insulator materials, as well as permanent air injection and ventilation have been shown to produce an essential sink for ions in the BACCARA chamber; while the importance of this sink in the Roselend tunnel stays for a moment uncertain. The total area of the walls and other surfaces relative to the volume of the cavity is about twice less in the case of the Roselend tunnel than in the BACCARA chamber. Third, the mobility of ions created in the moist air of the Roselend tunnel will be likely different (up to few tens of percents) to that found in dry air of the BACCARA chamber. What is common for the two series of tests is a slight difference observed between the positive and negative conductivities with the negative conductivity being about 10–20% higher than the opposite one. Such difference is most likely caused by the different mobility of the ion species found in the Earth's atmosphere [see, e.g., *Shreve*, 1970].

7. Summary of Results

We have presented measurements performed with the two types of conductivity sensors in two environments which contain ^{222}Rn gas. In the first environment, the ^{222}Rn gas naturally escapes from fractured granitic rocks and then accumulated in the enclosed space of the Roselend tunnel and the adjacent inner room. ^{222}Rn activity concentration in this case is mainly controlled by the rock source and modulated by water motion as well as by air ventilation from outside the tunnel. In the other environment, the ^{222}Rn gas is generated with help of one of the radioactive sources accommodated in the BACCARA facility and selected gases can be injected at a given total pressure. The ^{222}Rn activity concentration in this case is controlled by the source choice and by the dilution of the gas injection. Quasi-stationary conditions can be achieved for the test duration up to tens of hours. Both environments are precious for testing the design and performances of the conductivity sensors, which are developed to work in atmospheres with an electric conductivity ranging between ~10^{-13} and 10^{-9} S m^{-1}. The main advantage of both environments is an abundant number of ions created by the ^{222}Rn decay chain. An increase of the ^{222}Rn activity concentration, natural or generated in the laboratory, comes with an increase of the ion concentration and, thus, of the electric conductivity of air. Performing measurements with the conductivity sensors in ^{222}Rn-rich air, we were able (i) to demonstrate the efficiency of the CS-2 design to shield the electrode measurements from the external electric field, (ii) to propose simple low-voltage electronics, (iii) to justify an analytical model that allows to calculate the electric conductivity of air from the measured coupling resistance, (iv) to find out the relationship between the

^{222}Rn activity concentration and air electric conductivity in quasi-stationary and non-stationary conditions, and (v) to estimate the ion mobility and the ion density of the light ions using measurements of two conductivity sensors in a CO_2 atmosphere at low pressure.

In addition, we developed an analytical model that allows (i) to fit the measurements of the conductivity sensors in the BACCARA chamber, (ii) to estimate the loss of alpha particles on the chamber walls at low atmospheric pressure and for different gases (N_2 and CO_2), and (iii) to calculate the ion sink on the chamber internal structures.

Wilkening and Watkins's model was used to interpret the temporal variation of the ^{222}Rn activity concentration observed in the inner room of the Roselend tunnel and to determine the ^{222}Rn exhalation flux from the walls and the rate of the air exchange between the inner room and the tunnel.

8. Conclusion

Radon-222-rich environments can be used to test newly developed instruments designed to measure the air electric conductivity and to validate their design and concept. The concept of the conductivity sensors is based on the classical time relaxation method. New elements of the CS-2 design are (i) isolation of the sensor sensitive part (electrode) from the external electric field and (ii) sensor miniaturization. Thanks to measurements in ^{222}Rn-rich environments, the efficiency of the conductivity sensor-2 design to shield the electrode measurements from the external electric field was proven and estimated. The proposed design lets a possibility to perform the measurements of the electric conductivity independently of the magnitude of the external electric field and to use simple low-voltage electronics.

The enhanced ionization rate produced by the ^{222}Rn and its progeny decay in a gas increases the ion concentration and thus the electric conductivity of this gas. However, the relationship between the ^{222}Rn activity concentration and the electric conductivity is not straightforward. The role of the ion sink and of the loss of alpha particles on the chamber walls and other internal structures were considered and quantified in this study.

A more sophisticated modeling of the conductivity sensors and detailed analysis of the sensor response in presence of different sources of air ionization will be the subject of upcoming work.

Acknowledgments
We thank J.-C. Sabroux (IRSN) and B. Sabot (CEA) for stimulating discussions and help in organizing and conducting the BACCARA campaign. The conductivity sensor engineering model developed in the frame of the ExoMars 2020 Lander mission was financially supported by CNES. We thank M. Viso (CNES) for his interest and encouragements.

References

Bé, M., V. Christé, C. Dulieu, X. Mougeot, V. Chechev, and F. Kondev (2013), Table of radio nuclides, 7-A, 14 -245, Bureau International des Poids et Mesures, ISBN 13 978-92-822-2248-5.

Bethe, H. A. (1930), Zur Theorie des Durchgangs schneller Korpuskularstrahlen durch Materie, *Ann. D. Phys.*, *5*, 325.

Cabane, M., P. Krien, G. Madelaine, and J. Bricard (1976), Mobility spectra of ions created in gases under atmospheric pressure, *J. Colloid Interface Sci.*, *57-2*, 289–300.

Harrison, R. G., and H. Tammet (2008), Ions in the terrestrial atmosphere and other solar system atmospheres, *Space Sci. Rev.*, *137*, 107–118.

Hõrrak, U., J. Salm, and H. Tammet (2000), Statistical characterization of air ion mobility spectra at Tahkuse Observatory: Classification of air ions, *J. Geophys. Res.*, *105*, 9291–9302, doi:10.1029/1999JD901197.

International Commission on Radiation Units and Measurements (ICRU) (1993), Stopping Power and Ranges for Protons and Alpha Particles (Report 49).

Jess, W. P., and J. Sadaukis (1957), Absolute energy to produce an ion pair by beta particles from S^{35}, *Phys. Rev.*, *107*, 766–771.

Lucas, H. F. (1957), Improved low-level alpha scintillation counter for radon, *Rev. Sci. Instrum.*, *28*(9), 680–683.

Michielsen, N., and V. Voisin (1999) Calibration of radon measuring instruments over a large range of activity concentration, Proc. of Radon in the living environment, Athens, 19–23 April.

Mozer, F. S., and R. Serlin (1969), Magnetospheric electric field measurements with balloons, *J. Geophys. Res.*, *74*, 4739–4754.

Park, S. H., H. O. Kim, Y. T. Han, S. B. Kwon, and K. W. Lee (2001), Wall loss rate of polydispersed aerosols, *Aerosol Sci. Technol.*, *35*, 710–717.

Perrier, F., P. Richon, and J.-C. Sabroux (2005), Modelling the effect of air exchange on ^{222}Rn and its progeny concentration in a tunnel atmosphere, *Sci. Total Environ.*, *350*, 136–150.

Picolo, J.-L., D. Pressyanov, P. Blanchis, N. Michielsen, D. Grassin, V. Voisin, and K. Turek (2000), A radon 222 metrological chain, From primary standard to field detectors, *Appl. Radiat. Isot.*, *52*, 427–434.

Pili, E., F. Perrier, and P. Richon (2004), Dual porosity mechanism for transient ground-water and gas anomalies induced by external forcing, *Earth Planet. Sci. Lett.*, *227*, 473–480.

Price, W. J. (1964), *Nuclear Radiation Detection*, pp. 2–13, McGraw-Hill, New York.

Richon, P., F. Perrier, J.-C. Sabroux, M. Trique, C. Ferry, V. Voisin, and E. Pili (2005), Spatial and time variations of radon-222 concentration in the atmospheres of a dead-end horizontal tunnel, *J. Environ. Radioact.*, *78*, 179–198.

Röttger, A., et al. (2006), Radon activity concentration—A Euromet and BIPM supplementary comparison, *Appl. Radiat. Isot.*, *64*(10-11), 1102–1107.

Seran, E., M. Godefroy, N. Renno, and H. Elliott (2013), Variations of electric field and electric resistivity of air caused by dust motion, *J. Geophys. Res., Space Physics*, *118*, 5358–5368, doi:10.1002/jgra.50478.

Shreve, E. L. (1970), Theoretical derivation of atmospheric ion concentrations, conductivity, space charge density, electric field and generation rate from 0 to 60 km, *J. Atmos. Sci.*, *27*, 1186–1194.

Trique, M., P. Richon, F. Perrier, J. P. Avouac, and J.-C. Sabroux (1999), Radon emanation and electric potential variations associated with transient deformation near reservoir lakes, *Nature*, *399*(6732), 137–141.

Wilkening, M. H., and D. E. Watkins (1976), Air exchange and ^{222}Rn concentration in the Carlsbad caverns, *Health Phys.*, *31*, 139–145.